

# Influence of functionalization type on controlled release of emodin from mesoporous silica

Suman Jangra<sup>1,2</sup> · Vinod Chhokar<sup>2</sup> · Vijay K. Tomer<sup>1</sup> · Ashok K. Sharma<sup>1</sup> · Surender Duhan<sup>1</sup>

Published online: 24 March 2016  
© Springer Science+Business Media New York 2016

**Abstract** Emodin drug was introduced into the porous mesochannels of ( $\gamma$ -chloropropyl)triethoxysilane (CPTES) and (3-aminopropyl)triethoxysilane (APTES) functionalized SBA-15 via a hydrothermal process. The pure, functionalized and drug loaded mesoporous materials were characterized by small angle X-ray powder diffraction, field scanning electron microscopy, high resolution transmission electron microscopy, nitrogen adsorption–desorption, Fourier transformed infrared spectra, and UV–visible spectrophotometry. The functionalization of mesoporous silica reduced the degree of crystallinity of the resulting material. High resolution transmission electron microscope images of the functionalized materials demonstrated the reservation of the hexagonal mesoporous structure of SBA-15. Pure, CPTES and APTES-functionalized mesoporous silica were employed as base materials for the controlled release of emodin drug. Drug loading results revealed that the loading capabilities largely depend on the specific surface area, and pore volume and pore diameter of the carrier matrix. Emodin drug release profiles were studied in phosphate buffered saline with pH 7.4, and outcomes specified that the drug release rate could be controlled by the surface CPTES and APTES-functionalized carrier matrices. Emodin loaded functionalized materials presented a lower release rate compared to that of the pure SBA-15. Emodin loaded APTES-functionalized SBA-15 presented the lowest release amount of 74.5 % even up to

60 h. These results propose that the functionalized mesoporous silica is a favorable drug carrier for accomplishing prolonged release time.

**Keywords** CPTES · APTES · Functionalized mesoporous silica · Controlled release · Emodin

## 1 Introduction

Over the past two decades plenty of research has been performed worldwide on controlled drug release systems [1] such as ordered mesoporous silica: SBA-15, SBA-16, and AMS-1 [2, 3]. Controlled drug release systems have the ability to maintain the actual concentration of drug at the target organic tissue, thereby yield various advantages compared to traditional dosage regimens, including reduced toxicity, improved therapeutic efficacy, sustained efficiency time and enhanced bioavailability [4, 5]. Generally, the controlled drug release systems consist of a matrix carrier and a drug. Initially, the drug is loaded into the matrix then it is allowed to release from the carrier matrix at a targeted site under appropriate conditions. To facilitate this, the drug carrier matrix must satisfy several conditions such as (1) site directing ability, (2) excellent biocompatibility, (3) good ability to load high amount of a drug along with zero possibility of premature release of the drug, (4) cell type or tissue specificity and (5) controlled drug release rate to accomplish an effective local concentration [6]. The mesoporous silica materials synthesized by ionic, nonionic and amphiphilic block copolymers have captivated a great interest due to their unique properties. However, an innovative property of mesoporous silica (or SBA-15) for controlled drug release was disclosed by Vallet-Regi [7] in 2001. Afterwards, many research groups

✉ Surender Duhan  
surender6561@gmail.com

<sup>1</sup> Nanomaterials Research Laboratory, Department of Materials Science and Nanotechnology, D. C. R. University of Science and Technology, Murthal, Sonapat 131039, India

<sup>2</sup> Department of Bio-Nanotechnology, G.J. University of Science and Technology, Hisar 125001, India

have worked on that novel application of SBA-15 [8–13] due to its auspicious properties including stable uniform mesoporous structure, large surface area and adjustable pore size with narrow distribution, large pore volume and exceptional biocompatibility. Furthermore, the adsorption of poorly soluble drugs onto SBA-15 with large surface zones is a growing approach for improving drug dissolution [14]. It was realized that drug loading and its release rate could be controlled up to a great extent by functionalization of mesoporous structures such as SBA-15. Song et al. [15] showed that aminopropyl-modified SBA-15 provided higher drug loading capability than that of neat SBA-15 material. In similar manner, Xu et al. [16] showed that an effective drug controlled release system can be developed using amino-functionalization of SBA-15 material. However, Wang et al. [17] revealed that the mesoporous SBA-15 can be modified using ( $\gamma$ -chloropropyl)triethoxysilane (CPTES).

In this work, an attempt has been made to develop an effective controlled drug release system using neat, amino-functionalized and CPTES-functionalized SBA-15 as drug carriers. A poorly water soluble drug such as Emodin (1,3,8-trihydroxy-6-methyl-9,10-anthraquinone) has been used as a model drug for loading and controlled release study. In-vitro emodin drug release profiles were investigated by directly soaking emodin-loaded SBA-15 powder material in phosphate buffered saline (pH 7.4). In this study, first time CPTES-functionalized SBA-15 is used as a support material for the controlled release of emodin. The proposed controlled drug release system in this study has a potential of achieving a prolonged release of water-insoluble drugs.

## 2 Experimental

### 2.1 Reagents

Pluronic P<sub>123</sub> [ethylene oxide–propylene oxide–ethylene oxide (EO<sub>20</sub>PO<sub>70</sub>EO<sub>20</sub>), Mw = 5800], tetraethoxy orthosilicate [(C<sub>2</sub>H<sub>5</sub>O)<sub>4</sub>Si, TEOS], (3-aminopropyl)triethoxysilane (98 %) (APTES), titanium tetra-chloride (TiCl<sub>4</sub>), ( $\gamma$ -chloropropyl)triethoxysilane (CPTES) and HCl (35 %) were supplied by Sigma-Aldrich, India. Emodin was generously gifted by RPG Life Sciences Ltd., Mumbai, India. Double deionized water was used throughout the experiments. All of the chemicals and solvents used in this study were of analytical grade.

### 2.2 Synthesis of pure SBA-15 matrix

Mesoporous silica (or SBA-15) was prepared by following our earlier reported work [18]. Initially 2 g triblock

copolymer, P<sub>123</sub> was dissolved in 70 ml distilled water at 40 °C under high acidic conditions produced by the addition of 10 ml HCl (2 M). A clear solution was achieved after 3 h of continuous mechanical stirring of the solution. Then, 4.8 ml TEOS was added to the above mentioned solution followed by continuous stirring for another 24 h at 40 °C. Thereafter, the solution was transferred to a Teflon lined stain-less steel autoclave and hydrothermally treated at 100 °C for 24 h. At room temperature, the solid products were filtered, washed and dried at 70 °C. Finally, the solid product was calcined at 600 °C with a heating rate of 1 °C/min for 4 h in air to remove organic templates and to obtain pure mesoporous powder form SBA-15.

### 2.3 Synthesis of CPTES-functionalized SBA-15

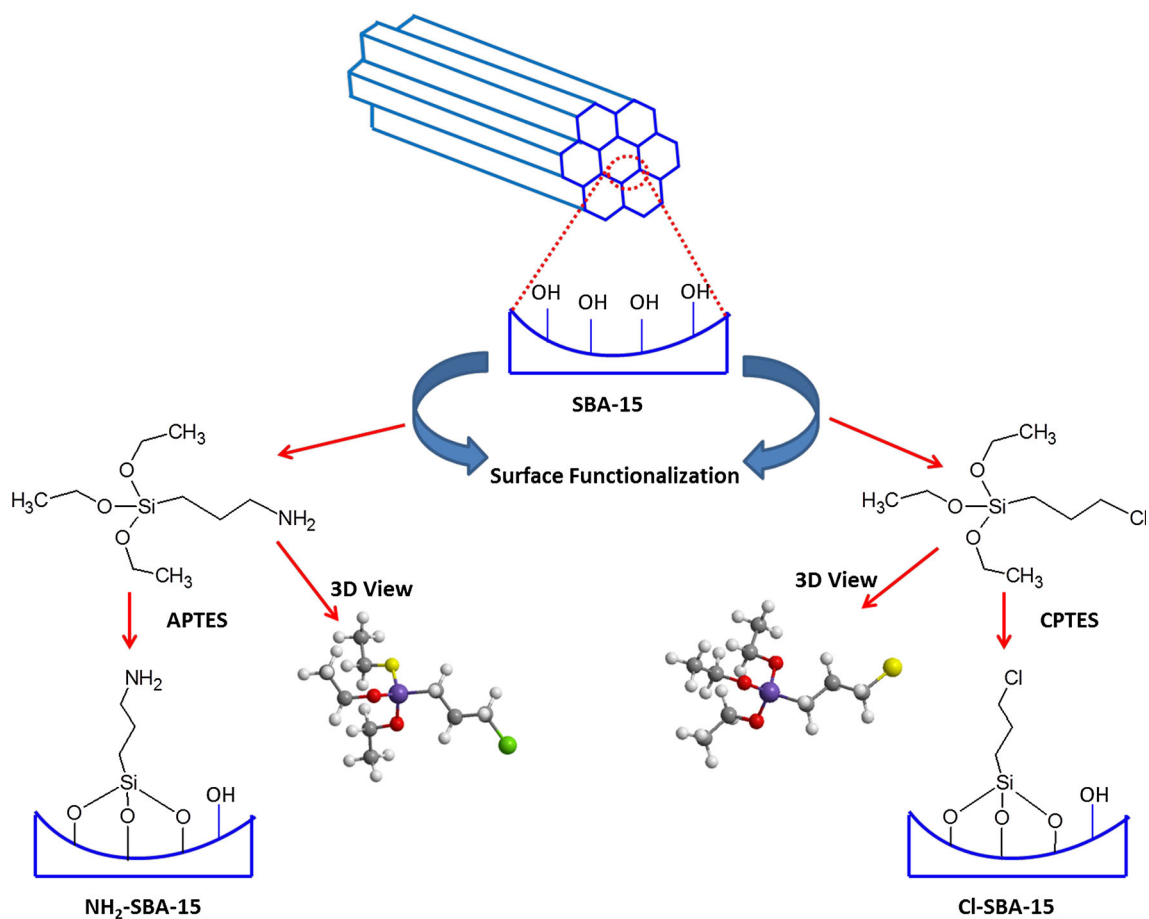
( $\gamma$ -chloropropyl)triethoxysilane (CPTES) was used as a silylation reagent in order to prepare the CPTES-functionalized SBA-15 [17]. Initially, 2 g of CPTES was mixed to 50 mL of dry toluene and then 2 g of mesoporous silica SBA-15 powder was mixed in it. The mixture was kept at 100 °C and continuously stirred for 48 h in a nitrogen atmosphere under reflux conditions. The resulting powder was filtered and washed with toluene (30 mL), ethanol (30 mL), and diethyl ether (30 mL), respectively. For ease in writing, the resulting powder is designated as SBA-Cl (Scheme 1).

### 2.4 Synthesis of APTES-functionalized SBA-15

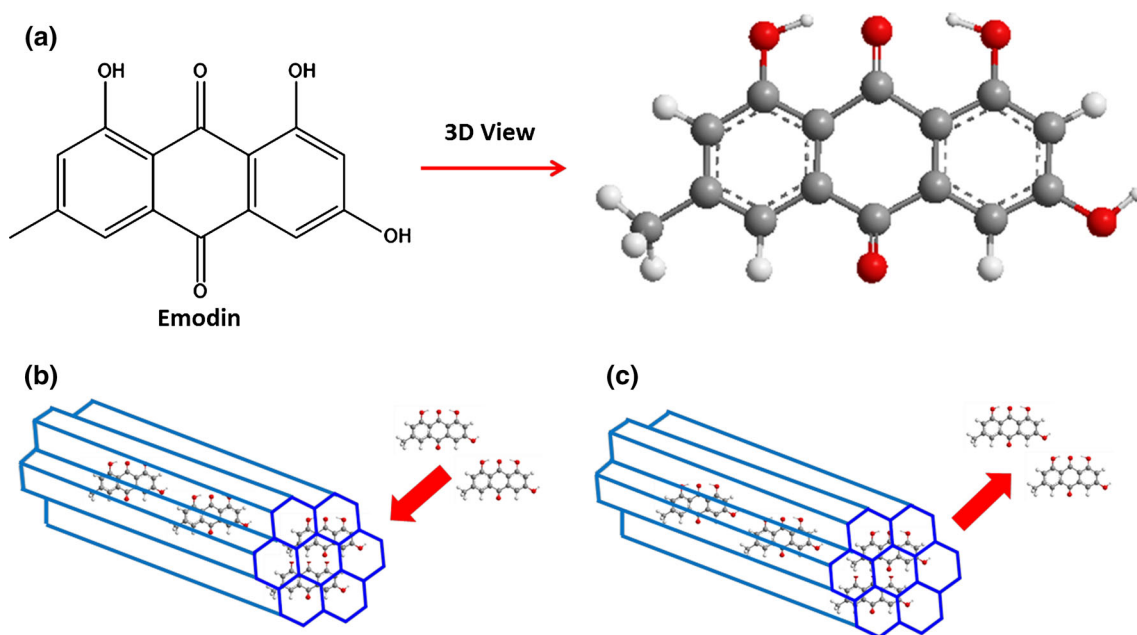
For synthesis of functionalized SBA-15, a method similar to obtain the pure SBA-15 was followed, except that APTES was also added to the mixture as soon as addition of TEOS. Afterwards, the mixture was pre-hydrolyzed for about 2 h [19], and then APTES was added dropwise into the solution. The molar composition of the mixture was 0.9 TEOS:0.1 APTES:5.71 HCl:0.017 P<sub>123</sub>:192 H<sub>2</sub>O. The resulting mixture was continuously stirred for 24 h at 40 °C prior to its transfer into a Teflon lined stain-less steel autoclave and hydrothermally treated at 100 °C for 24 h. At room temperature, the solid products were filtered, washed and dried at 70 °C. Later, the surfactant was removed by adding 1 g of the as-synthesized sample into 300 mL of ethanol and was Soxhlet refluxed for 24 h [16]. The resultant white powder was obtained after drying at ambient conditions. For ease in writing, the resulting powder is designated as SBA-AP (Scheme 1).

### 2.5 Drug loading

Emodin was taken as a model drug to estimate the loading and release performance of SBA-15 and the functionalized SBA-15 (Scheme 2a). About 200 mg of the support was



**Scheme 1** CPTES and APTES-functionalization of SBA-15



**Scheme 2** Emodin drug loading and release scenario

drenched in 50 mL of emodin-ethanol solution ( $0.5 \text{ mg mL}^{-1}$ ) and then continuously stirred for 24 h at ambient temperature without allowing solvent evaporation. The emodin-loaded sample was filtered and dried at ambient temperature. The filtrate (1.0 mL) was appropriately diluted to calculate the drug concentration with the help of a UV-vis spectrophotometer at a wavelength of 217 nm. The drug loading concentration was determined in accordance with the mass balance of emodin solution prior and after stirring using Eq. (1).

$$P_E = \frac{C_i - C_f}{W} \times V \quad (1)$$

where,  $P_E$  is loading content of emodin engrossed into the matrix ( $\text{mg g}^{-1}$ , mg emodin per gram SBA-15),  $C_i$  and  $C_f$  are the initial and final contents of the emodin in the solution ( $\text{mg mL}^{-1}$ ) respectively.  $V$  is volume of the solution (mL) and  $W$  is weight of the SBA-15 (g). The drug loading into pure mesoporous (SBA-15), CPTES-functionalized SBA-15 (SBA-Cl) and APTES-functionalized SBA-15 (SBA-AP) materials was accomplished following the same procedure (Scheme 2b). For ease in writing, the emodin drug loaded samples were designated as SBA-Cl-Em and SBA-AP-Em respectively.

## 2.6 Drug release

In vitro emodin release from the SBA-15 was executed as follows. Initially, 40 mg of the sample was engrossed in 50 mL of PBS with gentle stirring at  $37 \pm 0.5 \text{ }^\circ\text{C}$ . About 5 mL of the mixture was removed at pre-decided time intervals and instantaneously replaced by 5 mL of fresh PBS. The removed 5 mL mixture was filtered and examined using a UV-vis spectrophotometer. Since some portion of the drug loaded sample was extracted from the release mixture so the corresponding portion of the drug can't be reflected for next sampling. Hence, a corrected method [20] was employed to determine the real content of the drug released from the drug loaded composite material (Scheme 2c), using Eq. (2).

$$C_{t\text{-corrected}} = C_t + \frac{v}{V} \sum_0^{t-1} C_t \quad (2)$$

where,  $C_{t\text{-corrected}}$  ( $\text{mg mL}^{-1}$ ) is the real concentration of emodin released at time  $t$ ,  $C_t$  is the content of release fluid measured by UV-visible spectrometer ( $\text{mg mL}^{-1}$ ) sampled at time  $t$ ,  $v$  the sampled volume taken at specific time interval (mL), and  $V$  is the total volume of release fluid (mL).

The actual quantity of emodin released from mesoporous SBA-15 material in the release fluid was determined using Eq. (3).

$$A_{t\text{-released}} = \frac{C_{t\text{-corrected}} \times V}{P_E} \times 100 \quad (3)$$

where  $A_{t\text{-released}}$  is the actual concentration of released emodin at time  $t$  (%),  $C_{t\text{-corrected}}$  is the content of released emodin at time  $t$ ,  $V$  is the total volume of release fluid, and  $P_E$  is loading content of emodin engrossed into the matrix.

## 2.7 Characterization

Powder small-angle X-ray diffraction (SAXRD) patterns were obtained on a Bruker D8 advance diffractometer using Cu-K $\alpha$  as target material ( $\lambda = 0.15418 \text{ nm}$ ) to determine the crystallinity of the samples. The signals were recorded from  $0.5^\circ$  to  $5^\circ$  with a scanning step of  $0.01^\circ$  and a time per step of 10 s. Morphology of samples was characterized by field emission scanning electron microscope (FESEM, FEI QUANTA 200F) and high resolution transmission electron microscope (HRTEM, TECNAI G20) operated at an accelerating voltage of 200 kV. Fourier transform infrared spectra of samples were obtained by accumulating scans on a Perkin-Elmer BX II spectrophotometer with potassium bromide (KBr) pellets, in the range of  $4000\text{--}400 \text{ cm}^{-1}$ . At a temperature of  $-196 \text{ }^\circ\text{C}$ , a Micrometrics Tri-Star analyzer was used to obtain Nitrogen ( $\text{N}_2$ ) adsorption-desorption isotherms. Using the isotherms specific surface area and pore channel structural parameter were calculated by following BET (Brunner-Emmett-Teller) method [21]. The pore size distribution and pore volume were determined using the Barrett-Joyner-Halenda (BJH) model [22]. The calculations were based on the amount of nitrogen adsorbed which was recognized from nitrogen adsorption-desorption isotherms of each sample. The content of emodin in functionalized and non-functionalized SBA-15/emodin composite material was determined using UV-visible spectrophotometry (Shimadzu UV-2450, Milton Keynes, UK) [23]. The UV-vis Spectrophotometer, equipped with 1.0 cm cell was used for spectrophotometric determination of the content of emodin using Eq. (1).

## 3 Results and discussion

### 3.1 Structure of pure SBA-15, functionalized SBA-15 and drug loaded mesoporous material

#### 3.1.1 SAXRD analysis

Figure 1 displays the SAXRD pattern of the six samples. The pure SBA-15 (curve a) and SBA-Em (curve b) noticeably reveal one well-resolved diffraction peak of (100), and two weak diffraction peaks of (110) and (200) with d-spacing value is  $\sim 93.1 \text{ \AA}$ . These three peaks at

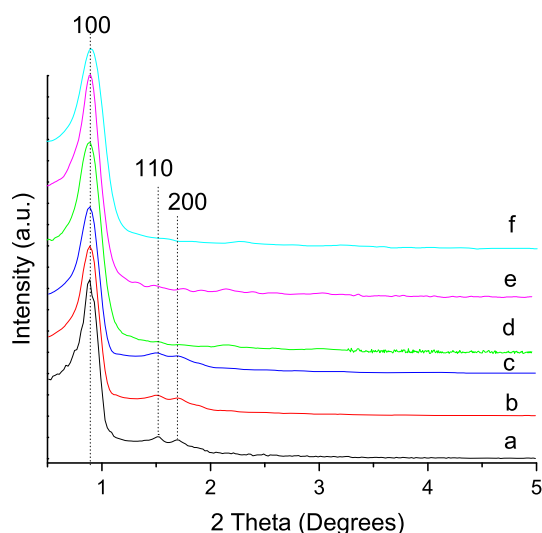


**Fig. 1** SAXRD patterns of *a* SBA-15, *b* SBA-Em, *c* SBA-Cl, *d* SBA-AP, *e* SBA-Cl-Em and *f* SBA-AP-Em

0.9°, 1.52° and 1.7° respectively correspond to a highly ordered, p6 mm hexagonal symmetry of a mesoporous structure (SBA-15) in agreement with the data reported in the literature [2]. A slight change in form of broadening of peaks (curve b) may be due to loading of the drug into the mesoporous material. However, the loading of drug does not disturb the actual structure of the SBA-15. Grafting CPTES in SBA-15 (curve c) does not change the characteristic  $2\theta$  values of diffraction peaks of (100), (110) and (200). But, the decrease in the intensity of two weak peaks indicates slight change in the structure of the mesoporous material which may be attributed to the creation of a functional molecule layer due to the condensation between CPTES and hydroxyl group of SBA-15 [17]. Grafting APTES in SBA-15 (curve d) results in loss of two weak peaks of (110) and (200) indicating a weak ordering in mesostructure. Only one wide (100) diffraction peak is detected, which indicates very poor ordered mesoporous structure of the SBA-15 material. This may be ascribed to protonation of APTES under strong acidic conditions and which also affect the self-assembly of the triblock copolymer (P<sub>123</sub>) and silica precursor. Furthermore, the protonated amine groups may actively interact with ethoxy groups of TEOS via hydrogen bonding, which inhibits the hydrolysis and condensation of the silane group [24]. The drug loaded CPTES and APTES functionalized SBA-15 samples (curve e and f) reveal only one wide (100) diffraction peak not the other two peaks, this may have happened due to the coupling of drug with the chloropropyl and amine groups occur inside the channels of composites SBA-Cl and SBA-AP respectively. Because, anchoring of noticeable amount of drug within channels of mesoporous structure reduces the scattering contrast of amorphous

silica wall [17]. Additionally, two distinct weak (110) and (200) diffraction peaks in the XRD pattern of the SBA-Em composite material (curve b) verifies the ordered mesoporous structure is not destroyed by the drug loading.

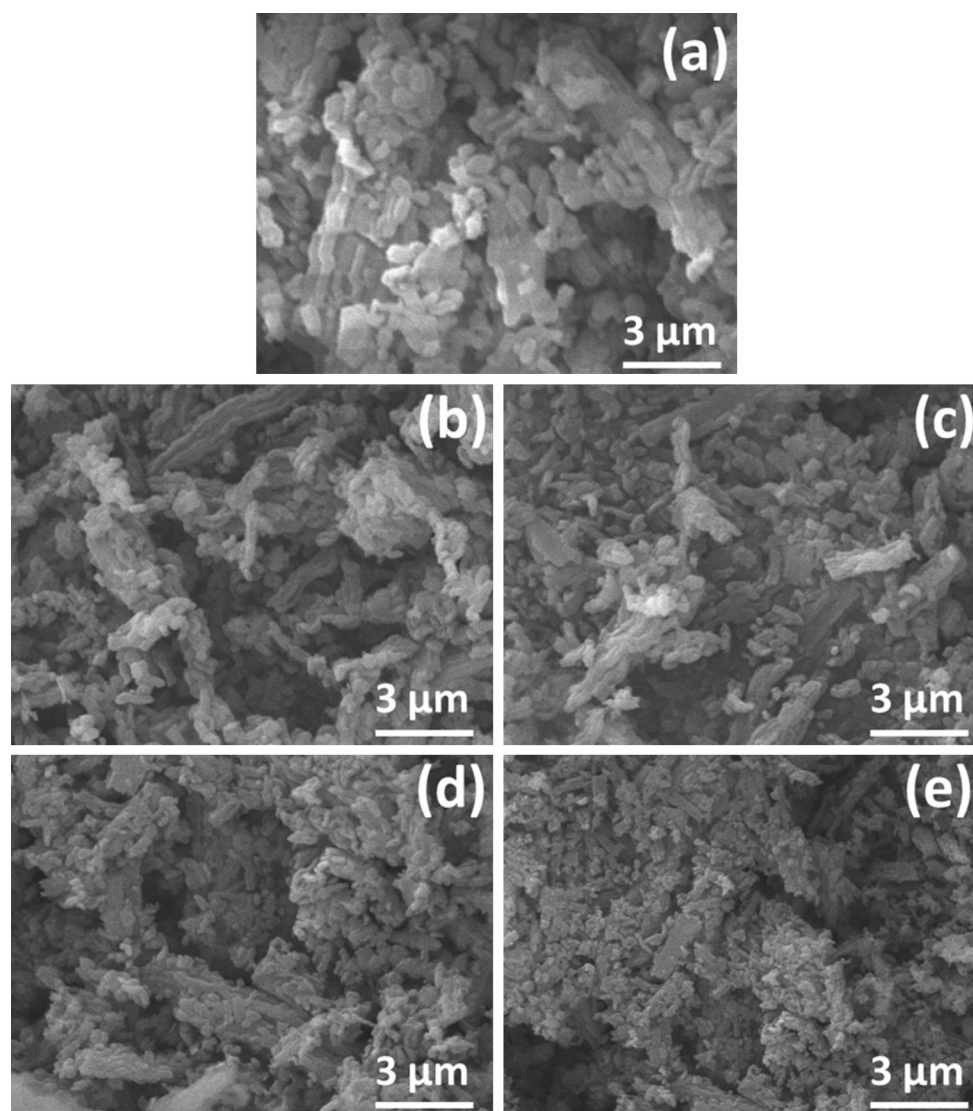
### 3.1.2 SEM analysis

FESEM micrographs of SBA-15, SBA-Cl, SBA-AP, SBA-Cl-Em and SBA-AP-Em are shown in Fig. 2. Microstructure of SBA-15 elucidates (Fig. 2a) rod-like domains aggregated to wheat-like structures. Such types of microstructures consist of large fibrous structures generally ranging from 2 to 5  $\mu\text{m}$  in length and 0.5 to 2  $\mu\text{m}$  in diameter. The typical wheat-like structures of packed agglomerates also consist of several short-rod domains with comparatively uniform sizes of 1–2  $\mu\text{m}$  in length and 0.2–0.7  $\mu\text{m}$  in diameter [25]. Such type of morphology for weakly trapezoidal, wheat grain-like particles has already been established to have long-range mesoporous channels with 2D-hexagonal structure [26]. The FESEM microstructures show. Generally, the morphology of mesoporous structure SBA-15 depends on various parameters such as pH, co-surfactants, temperature, electrolytes and swelling agents, etc. [27]. The morphology of SBA-Cl (Fig. 2b) is almost similar to that of the mesoporous SBA-15. The microstructure of SBA-Cl also shows rod-like domains accumulated to wheat-like structures, but the length of domains appears longer and diameter seems shorter compared to the domains observed in the case of SBA-15. This change in the morphology of the material may be due to the introduction of CPTES into the pre-hydrolyzed SBA-15 mixture. The morphology of SBA-AP (Fig. 2c) is somewhat different from that of the mesoporous SBA-15. The microstructure of SBA-AP reveals less agglomerated wheat-like structures except few rod-like packed domains accumulated to wheat-like structures. Also the average size of less agglomerated wheat-like structures is 3–4 times smaller than that of the SBA-15. This noticeable change in the morphology of the material may happens due to the addition of APTES into the SBA-15 mixture during synthesis. The morphologies of SBA-Cl-Em (Fig. 2d) and SBA-AP-Em (Fig. 2e) are reasonably different from those of the SBA-Cl, SBA-AP and SBA-15, respectively. The microstructures of SBA-Cl-Em and SBA-AP-Em presenting integrated short-rod units with further densely packed macrostructures of small amorphous units. This significant change in the morphologies of the materials occurs due to loading of emodin drug in CPTES and APTES functionalized mesoporous material.

### 3.1.3 TEM analysis

HRTEM micrographs of the pure SBA-15, SBA-Cl, SBA-AP, SBA-Cl-Em and SBA-AP-Em, respectively are

**Fig. 2** FESEM images of **a** SBA-15, **b** SBA-Cl, **c** SBA-AP, **d** SBA-Cl-Em and **e** SBA-AP-Em

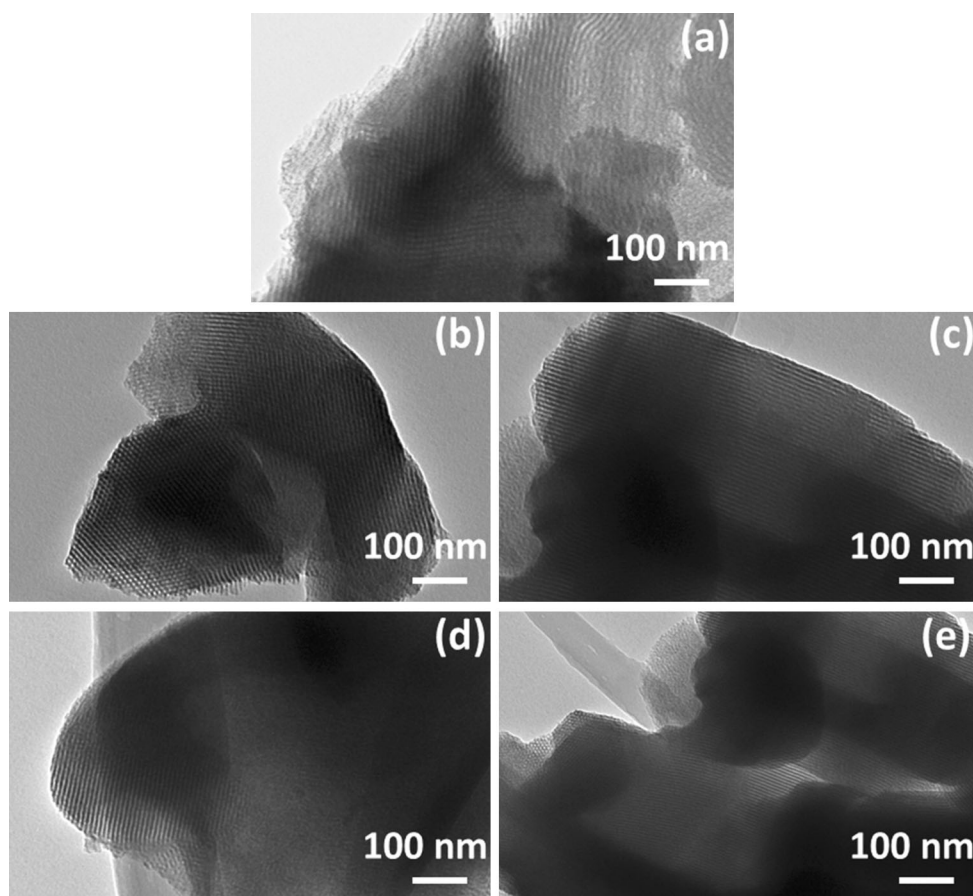


compared in Fig. 3. The micrograph of SBA-15 (Fig. 3a) clearly elucidates well-arranged hexagonal arrays of cylindrical nano-pores along the long axis, which is hitherto observed from the SAXRD patterns. The mesoporous SBA-15 reveals 2-dimensional hexagonal,  $p6mm$  structures accompanied by relatively uniform cylindrical pores of equal widths to effectively accommodate emodin. The mesochannels in the rod-like domains are along the long axis [25] and also the mesochannels of different domains are not connected with each other.

The diameter of mesochannels is less than 10 nm. In the micrograph, the different orientations of mesochannels are due to the presence of more than one rod-like domain at the same location. The HRTEM micrographs of SBA-Cl (Fig. 3b) and SBA-AP (Fig. 3c) also have well-arranged hexagonal arrays of mesochannels along the long axis, signifying that the 2D-hexagonal mesoporous structure is

preserved during the functionalization process. The mesh like structure revealed by SBA-Cl (Fig. 3b) is due to the presence of two rod-like domains at the same location and long-axis of both are perpendicular to each other. In this study, the HRTEM images specify that the variation in morphologies of the functionalized materials is due to different functionalization agents like CPTES and APTES. The HRTEM micrographs of SBA-Cl-Em (Fig. 3d) and SBA-AP-Em (Fig. 3e) reveal that well-arranged hexagonal arrays of mesochannels cannot be clearly identified inside the material. However, at the edges, a regular periodic arrangement of mesochannels can be distinguished. Therefore, the material may be regarded to present worm-like structural pores, on the other hand it preserve some hexagonally arranged mesochannels in its domain. The encapsulation of foreign material (emodin drug) into the mesochannels of SBA-15 does not change its hexagonal

**Fig. 3** HRTEM images of **a** SBA-15, **b** SBA-Cl, **c** SBA-AP, **d** SBA-Cl-Em and **e** SBA-AP-Em



structure to a large extent. But from the micrographs (Fig. 3d, e), there is no existence of combined emodin drug particles and therefore, it may be concluded that the drug is consistently distributed into the mesochannels of SBA-15.

### 3.1.4 FTIR spectra

The functionalization of silica framework may be understood by the Fourier transform infrared (FTIR) data. The FTIR spectra of SBA-15, SBA-Cl and SBA-AP are shown in Fig. 4. The typical Si–O–Si bands at 1634, 1086, 802 and 460  $\text{cm}^{-1}$ . (Figure 4a) correspond to the condensed network of silica in case of the pure SBA-15, which is also supported by the XRD spectra, FESEM and HRTEM results. A relatively broad band at 3447  $\text{cm}^{-1}$  is correspond to silanol stretching vibration and moreover, because of the presence of OH group of water molecules into mesochannels of SBA-15 [28]. For all the mesoporous silica samples, a broad band at 1086  $\text{cm}^{-1}$  is attributed to Si–O asymmetric stretching [29]. Also the presence of any weak peaks in the range 940–965  $\text{cm}^{-1}$  corresponds to the non-condensed Si–OH groups [30]. The silanol groups of pure SBA-15 presents a characteristic weak peak at 964  $\text{cm}^{-1}$ . Because of the functionalization of SBA-15 with CPTES

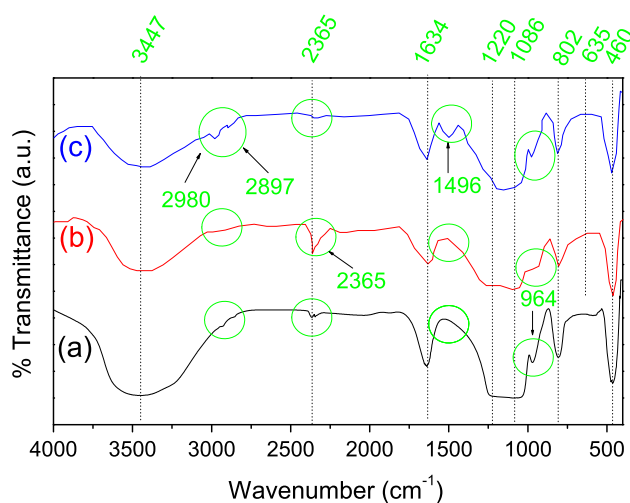


**Fig. 4** FTIR spectra of **a** SBA-15, **b** SBA-Cl and **c** SBA-AP

(Fig. 4b), the weak peak declines and even disappears, signifying the formation of –Si–O– bands. This happens due to the reaction between the silanol groups of SBA-15 and  $(\text{C}_2\text{H}_5\text{O})_3\text{Si}$ – groups of silylation reagent [17]. Therefore, weaker vibration intensity in the FTIR spectra is observed possibly due to decrease of silanol groups. The

characteristic bands at 2897 and 2980  $\text{cm}^{-1}$  associated with C-H stretching (Fig. 4c) [31]. A specific band at 1496  $\text{cm}^{-1}$  could be possibly attributed to the deformations of the  $\text{NH}^{3+}$  moiety [32]. This specific band is observed for functionalized material but not in pure SBA-15. These typical bands authorize that aminopropyl groups of APTES have been successfully incorporated into the pure SBA-15. This can be easily perceived that almost each infrared signal of pure SBA-15 is exists in the infrared spectra of functionalized SBA-15 materials (Fig. 4b, c). That means the functionalization process does not destroy the main structure of SBA-15.

### 3.1.5 Nitrogen adsorption–desorption isotherms

Nitrogen ( $\text{N}_2$ ) adsorption–desorption isotherms are very effective to reveal the surface properties such as specific surface area, pore size distribution and pore volume of a mesoporous material. The low temperature  $\text{N}_2$  adsorption–desorption isotherms of SBA-15, SBA-Cl and SBA-AP are shown in Fig. 5. The corresponding BJH pore size distributions of these samples are shown in Fig. 6. All three samples display a classic irreversible type IV isotherm with clear H1 type hysteresis loop, which is characteristic of mesoporous materials with hexagonal cylindrical mesochannels with open pores [33, 34]. It is observed that the incorporation of CPTES during the synthesis process does not significantly modify the structure of mesoporous silica material. Whereas the introduction of APTES results in a less-sharp isotherm compared to SBA-15 and SBA-Cl, but it may still be categorized as type IV isotherm [35]. Such change in isotherm suggests that the functionalized moieties are inserted into the pores of the SBA-15 and up to certain extent disrupt the structure of the mesoporous

material, which is in decent agreement with the SAXRD patterns and HRTEM result as shown in Figs. 1 and 3, respectively. In case of SBA-Cl and SBA-AP, the amount of nitrogen uptake drops because of the shrinkage in the mesopore volume and also results in the decline in mesopore size as revealed by the corresponding pore size distribution curves in Fig. 6. Detailed textural properties of SBA-15, SBA-Cl and SBA-AP are shown in Table 1, which demonstrates that the textural factors of different materials are quite dissimilar. The pure SBA-15 has the maximum surface area (737  $\text{m}^2/\text{g}$ ), pore volume (0.94  $\text{cm}^3/\text{g}$ ) and pore diameter (9.4 nm). All the three parameters such as specific surface area, pore volume, and pore diameter determined by  $\text{N}_2$  adsorption–desorption isotherms decrease with the functional CPTES and APTES moieties. The SBA-AP reveals the smallest surface area 575  $\text{m}^2/\text{g}$ , pore volume (0.69  $\text{cm}^3/\text{g}$ ) and pore diameter (6.4 nm), signifying that APTES has a higher detrimental effect compared to CPTES on the mesostructured formation of functionalized materials.

## 3.2 Drug loading and release

### 3.2.1 $\text{N}_2$ adsorption–desorption isotherms

$\text{N}_2$  adsorption–desorption isotherms with the corresponding pore size distribution curves of SBA-15-Em, SBA-Cl-Em and SBA-AP-Em are shown in Figs. 7 and 8, respectively. All three samples demonstrate classic IV isotherms with H1 type hysteresis loops with a narrow pore size distribution, almost similar to the pure and functionalized mesoporous materials before emodin drug loading (Figs. 5, 6). This specifies that the mesoporous structure and pore

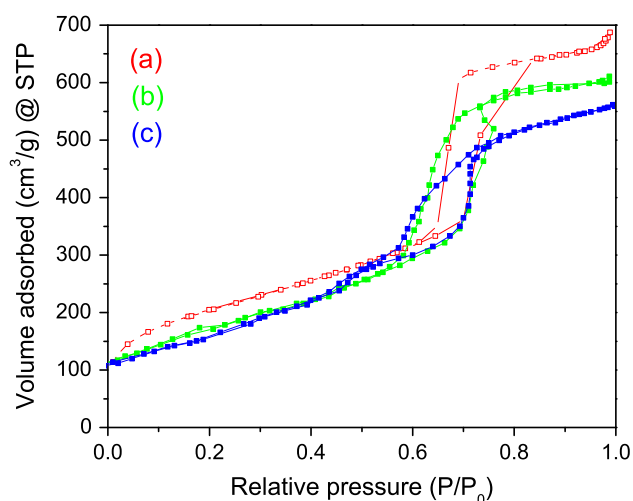


**Fig. 5**  $\text{N}_2$  adsorption–desorption isotherms of *a* SBA-15, *b* SBA-Cl and *c* SBA-AP

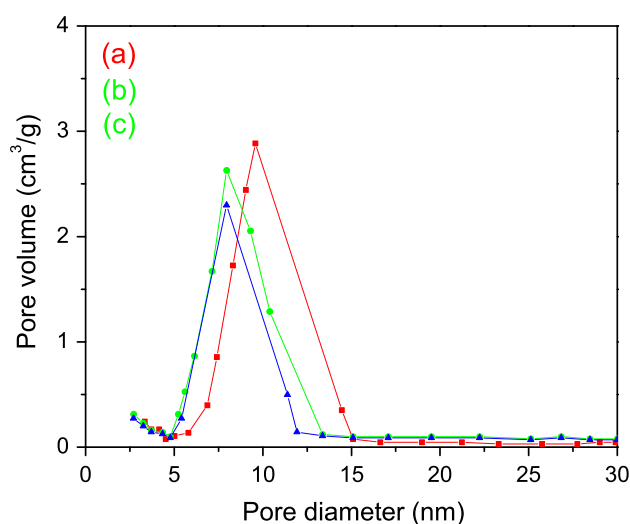


**Fig. 6** BJH pore size distribution curves of *a* SBA-15, *b* SBA-Cl and *c* SBA-AP



**Table 1** Surface area ( $S_{BET}$ ), pore volume ( $V_p$ ), and pore diameter ( $D_p$ ) of pure SBA-15 and functionalized SBA-15

Sample	$S_{BET}$ (m <sup>2</sup> /g)	$V_p$ (cm <sup>3</sup> /g)	$D_p$ (nm)
SBA-15	737	0.94	9.4
SBA-Cl	645	0.89	8.8
SBA-AP	575	0.69	6.4

**Table 2** Surface area ( $S_{BET}$ ), pore volume ( $V_p$ ), and pore diameter ( $D_p$ ) of drug loaded SBA-15 and functionalized SBA-15

Sample	$S_{BET}$ (m <sup>2</sup> /g)	$V_p$ (cm <sup>3</sup> /g)	$D_p$ (nm)
SBA-15-Em	723	0.90	8.7
SBA-Cl-Em	617	0.82	8.2
SBA-AP-Em	543	0.54	5.8

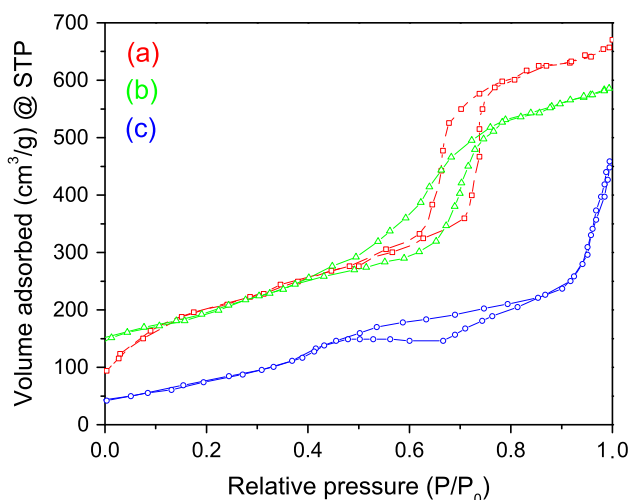


**Fig. 7** N<sub>2</sub> adsorption–desorption isotherms of *a* SBA-15-Em, *b* SBA-Cl-Em and *c* SBA-AP-Em

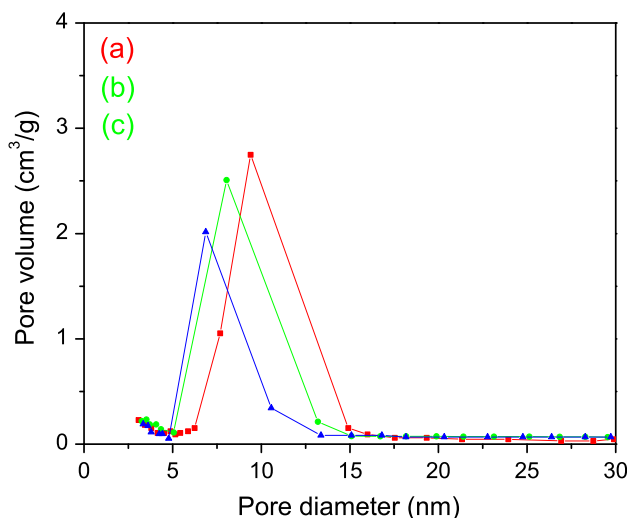


**Fig. 8** BJH pore size distribution curves of *a* SBA-15-Em, *b* SBA-Cl-Em and *c* SBA-AP-Em

shape of the pure and functionalized materials endure unaffected even after emodin drug loading. Also, the adsorbed quantity of N<sub>2</sub> seems to decline possibly due to

the drug loading, which indicates that the structural parameters of drug loaded samples marginally decreases compared to the corresponding without loaded samples of SBA-15. Detailed textural properties of SBA-15, SBA-Cl and SBA-AP are shown in Table 2. All the three parameters such as specific surface area, pore volume, and pore diameter of SBA-15-Em, SBA-Cl-Em, and SBA-AP-Em reduces compared to the corresponding without loaded samples of SBA-15, signifying that emodin drug molecules are loaded into the mesochannels of the mesoporous materials without pore plugging.

### 3.2.2 Drug loading

Generally, various factors such as specific surface area, pore size, pore volume etc. significantly affect the loading capacity of a drug in a mesoporous matrix. This is already verified by others that if the surface area and pore size of a mesoporous material decreases then lower loading of drug occurs [36, 37]. In this study, the amount of drug loaded into SBA-15 is comparable to that loaded into CPTES-functionalized SBA-15, signifying that functionalization of mesoporous SBA-15 by CPTES has nominal effect on the drug loading capacity. The emodin drug loading amount in pure and functionalized mesoporous matrices is illustrated in Table 3.

It is observed that the pure SBA-15 has the highest drug loading capacity about 8.23 mg/g due to its largest specific surface area and pore size. However, the CPTES functionalized SBA-15 has the drug loading amount of 7.87 mg/g, which is slightly less than that of the pure SBA-15. This indicates the drug loading amount declines due to decrease in specific surface area and pore size of the mesoporous material after functionalization by CPTES. But, the drug loading amount in APTES functionalized SBA-15 is lowest (6.41 mg/g), signifying that the surface

**Table 3** Loading amount of emodin drug in pure and functionalized mesoporous matrices

Sample	$P_E$ (mg/g)
SBA-15-Em	8.23
SBA-Cl-Em	7.87
SBA-AP-Em	6.41

area, pore size and pore volume of mesoporous material have a significant effect on drug loading.

### 3.2.3 Drug release

Since the molecular size of emodin drug less than 1 nm, so it can easily fit inside the pores of mesoporous SBA-15. Subsequently, the interaction between the drug and mesoporous material inside the pores is mainly depend on the occurrence of the –NH group via hydrogen bonding with free silanol groups on the surface of mesoporous material. In vitro drug release was employed in PBS with pH 7.4 to estimate the release profiles of the drug from the SBA-15. In vitro cumulative release profiles of emodin from the pure SBA-15, CPTES and APTES-functionalized SBA-15 are shown in Fig. 9. All three samples showing fast initial drug release rates, which can be denoted to as the “burst release. Over the range of 0.25–3 h, the sustained emodin drug release rate accelerated and a released amount of 76.74 % achieved. 48 h later, the drug release from SBA-15 was ultimately finished with a release amount of 98.19 % in case of SBA-15-Em. However, the drug release was comparatively slow in case of the functionalized materials. The SBA-CI-Em and SBA-AP-Em samples show slow release rates, signifying that the drug release can be controlled by functionalization of mesoporous SBA-15 with CPTES and APTES. The SBA-CI-Em sample reveals low release amount of emodin (91.7 %) even up to 60 h. But, the SBA-AP-Em sample reveals the lowest release amount of emodin (74.5 %) even up to 60 h. This behavior indicates that the drug release from long and bent mesochannels happens more slowly compared to the amorphous pores [38]. Several parameters like surface-

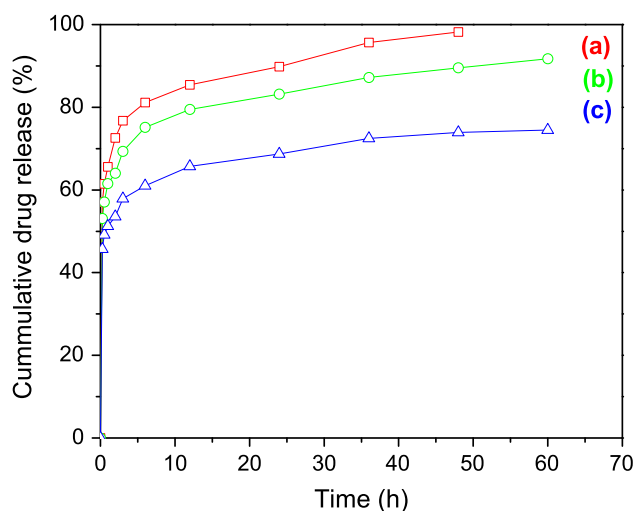


**Fig. 9** Emodin drug release profiles of *a* SBA-15-Em, *b* SBA-CI-Em and *c* SBA-AP-Em

interactions, ionic bond reactions and hydrogen bonding effects between emodin drug molecules and the surface of CPTES and APTES-functionalized SBA-15 matrix seem to be strong, which is responsible for reduction in drug release rate as well as prolonged release time. Thus, it can be inferred that the CPTES and APTES-functionalization of the mesoporous SBA-15 material efficiently delayed the release of emodin drug.

## 4 Conclusions

Functionalization of mesoporous silica materials were successfully accomplished by the CPTES and APTES materials via a hydrothermal process. The pure and functionalized silica materials were used as base matrices for loading and release of the water-insoluble emodin drug. The functionalization of SBA-15 reduced the degree of crystallinity of the base material. The results of HRTEM show that the mesoporous structure of SBA-15 is stable even after the surface functionalization by CPTES and APTES. The modification of the surface of SBA-15 leads to the better interaction of the drug with the carrier matrix. The loading amount of emodin adsorbed on mesoporous SBA-15 reduced due to the functionalization which also responsible for reduced specific surface area and pore size. The drug release profiles of pure and functionalized SBA-15 materials revealed a “Burst release” phenomena until the sixth hour of release. Emodin loaded into the functionalized silica materials revealed a lower release rate compared to that of the pure SBA-15, signifying that the surface functionalization of SBA-15 could efficiently delay the drug release. Particularly, the SBA-AP-Em material presented the lowest release rate about 74.5 % even up to 60 h. These results offer auspicious perspectives of functionalized mesoporous silica materials for future applications in drug delivery systems.

**Acknowledgments** Authors are grateful to UGC, New Delhi (Grant No. 41-997/2012(SR)) for providing financial assistance.

## References

1. J.S. Beck, J.C. Vartuli, W.J. Roth, M.E. Leonowicz, C.T. Kresge, K.D. Schmitt, C.T.W. Chu, D.H. Olson, E.W. Sheppard, J. Am. Chem. Soc. **114**, 10834 (1992)
2. S. Jangra, P. Girotra, V. Chhokar, V.K. Tomer, A.K. Sharma, S. Duhan, J. Porous Mat. (2016). doi:10.1007/s10934-016-0123-1
3. S. Che, A.E. Garcia-Bennett, T. Yokoi, K. Sakamoto, H. Kunieda, O. Terasaki, T. Tatsumi, Nat. Mater. **2**, 801 (2003)
4. P. Yang, Z. Quan, L. Lu, S. Huang, J. Lin, Biomaterials **29**, 692 (2008)
5. S. Wang, Microporous Mesoporous Mater. **117**, 1 (2009)
6. I.I. Slowing, J.L. Vivero-Escoto, C.-W. Wu, V.S.-Y. Lin, Adv. Drug Deliv. Rev. **60**, 1278 (2008)

7. M. Vallet-Regí, A. Rámila, R.P. del Real, J. Pérez-Pariente, *Chem. Mater.* **13**, 308 (2001)
8. B. González, M. Colilla, C.L. de Laorden, M. Vallet-Regí, *J. Mater. Chem.* **19**, 9012 (2009)
9. S.-H. Cheng, C.-H. Lee, C.-S. Yang, F.-G. Tseng, C.-Y. Mou, L.-W. Lo, *J. Mater. Chem.* **19**, 1252 (2009)
10. T.X. Bui, H. Choi, *J. Hazard. Mater.* **168**, 602 (2009)
11. Z. Xu, Y. Ji, M. Guan, H. Huang, C. Zhao, H. Zhang, *Appl. Surf. Sci.* **256**, 3160 (2010)
12. F. Qu, H. Lin, X. Wu, X. Li, S. Qiu, G. Zhu, *Solid State Sci.* **12**, 851 (2010)
13. Y. Yang, W. Song, A. Wang, P. Zhu, J. Fei, J. Li, *Phys. Chem. Chem. Phys.* **12**, 4418 (2010)
14. M. Van Speybroeck, V. Barillaro, T. Do Thi, R. Mellaerts, J. Martens, J. Van Humbeeck, J. Vermant, P. Annaert, G. Van den Mooter, P. Augustijns, *J. Pharm. Sci.* **98**, 2648 (2009)
15. S.-W. Song, K. Hidajat, S. Kawi, *Langmuir* **21**, 9568 (2005)
16. Y. Xu, C. Wang, G. Zhou, Y. Wu, J. Chen, *Appl. Surf. Sci.* **258**, 6366 (2012)
17. J.-Q. Wang, L. Huang, M. Xue, Y. Wang, L. Gao, J.H. Zhu, Z. Zou, *J. Phys. Chem. C* **112**, 5014 (2008)
18. V.K. Tomer, R. Malik, S. Jangra, S.P. Nehra, S. Duhan, *Mater. Lett.* **132**, 228 (2014)
19. Q. Wei, Z.-R. Nie, Y.-L. Hao, L. Liu, Z.-X. Chen, J.-X. Zou, *J. Sol-Gel. Sci. Technol.* **39**, 103 (2006)
20. K.A. Fisher, K.D. Huddersman, M.J. Taylor, *Chemistry* **9**, 5873 (2003)
21. V.K. Tomer, S. Jangra, R. Malik, S. Duhan, *Colloids Surf. A: Physicochemical and Engg. Aspects*, **466**, 160 (2015)
22. S.-C. Shen, W.K. Ng, L. Chia, J. Hu, R.B.H. Tan, *Int. J. Pharm.* **410**, 188 (2011)
23. Q.-Z. Zhai, *Mater. Sci. Eng. C* **32**, 2411 (2012)
24. X. Wang, Y.-H. Tseng, J.C.C. Chan, S. Cheng, *Microporous Mesoporous Mater.* **85**, 241 (2005)
25. A. Katiyar, S. Yadav, P.G. Smirniotis, N.G. Pinto, *J. Chromatogr. A* **1122**, 13 (2006)
26. H. Zhang, J. Sun, D. Ma, X. Bao, A. Klein-Hoffmann, G. Weinberg, D. Su, R. Schlögl, *J. Am. Chem. Soc.* **126**, 7440 (2004)
27. V. Meynen, P. Cool, E.F. Vansant, *Microporous Mesoporous Mater.* **125**, 170 (2009)
28. F.J.V.E. Oliveira, M.A. Melo, C. Airoidi, *Mater. Res. Bull.* **48**, 1045 (2013)
29. N. Navascués, C. Téllez, J. Coronas, *Microporous Mesoporous Mater.* **112**, 561 (2008)
30. H. Wang, X. Gao, Y. Wang, J. Wang, X. Niu, X. Deng, *Ceram. Int.* **38**, 6931 (2012)
31. B. Shi, Y. Wang, Y. Guo, Y. Wang, Y. Wang, Y. Guo, Z. Zhang, X. Liu, G. Lu, *Catal. Today* **148**, 184 (2009)
32. H. Kim, J.C. Jung, P. Kim, S.H. Yeom, K.-Y. Lee, I.K. Song, *J. Mol. Catal. A Chem.* **259**, 150 (2006)
33. D. Zhao, J. Sun, Q. Li, G.D. Stucky, *Chem. Mater.* **12**, 275 (2000)
34. G. Leofanti, M. Padovan, G. Tozzola, B. Venturelli, *Catal. Today* **41**, 207 (1998)
35. J. Rouquerol, F. Rouquerol, K.S.W. Sing, *Adsorption by Powders and Porous Solids: Principles, Methodology and Applications* (Academic Press, Cambridge, 1998)
36. P. Horcajada, A. Rámila, J. Pérez-Pariente, M. Vallet-Regí, *Microporous Mesoporous Mater.* **68**, 105 (2004)
37. F. Qu, G. Zhu, S. Huang, S. Li, J. Sun, D. Zhang, S. Qiu, *Microporous Mesoporous Mater.* **92**, 1 (2006)
38. Z. Jin, H. Liang, *J. Dispers. Sci. Technol.* **31**, 654 (2010)